

# Ghost orbits in the diamagnetic hydrogen spectrum using harmonic inversion

Benoît Grémaud and Dominique Delande

*Laboratoire Kastler Brossel, Université Pierre et Marie Curie, T12, E1  
4, place Jussieu, 75252 Paris Cedex 05, France*

(September 28, 2018)

## Abstract

The harmonic inversion method is applied in the case of the hydrogen atom in a magnetic field to extract classical information from the quantum photo-ionization cross-section. The study is made close to a saddle-node bifurcation for which the usual semi-classical formulas give diverging contributions. All quantities (actions, stabilities and Maslov indices) for real orbits above the bifurcation and for complex ghost orbits below the bifurcation, are found to be in excellent agreement with the modified semi-classical predictions based on a normal form approach.

PACS number(s): 31.15.Gy, 05.45.Mt, 03.65.Sq, 32.60.i

arXiv:chao-dyn/9907008v1 30 Jun 1999

## I. INTRODUCTION

The hydrogen atom in a strong magnetic field is one of the most appealing system to study chaotic effects in quantum mechanics: it has the minimum number of degrees of freedom, all quantum and classical properties can be computed in a exact way [1,2]. Some other systems share these properties, but the difference is that the chaotic regime for the magnetized hydrogen atom is also observed experimentally [3,4], which is the case of only few systems, as helium atom [5,6], hydrogen atom in a microwave field [7,8], resonant tunneling diode [9–11], experiments with cold atoms [12,13]. Chaos being defined at the classical level as exponential sensitivity on initial conditions, a major step in the understanding of chaos at the quantum level has been made trough the Gutzwiller trace formula, linking the quantum density of states to the classical periodic orbits of the system [14]. Later on, similar formula were derived to explain experimental observation, like photo-ionization cross-section, in terms of classical orbits (closed orbits in this case) [15,16].

The agreement between the numerical and experimental quantum results was found to be good, except for parameters (energy, magnetic field) too close to bifurcation points, at which the semi-classical amplitudes are diverging. However, these divergences have been later understood and classified using a normal form approach [4,17]. Especially, it emphasized the contribution of complex “ghost” [18] orbits (where both position and momentum are made complex quantities) in the photo-ionization cross-section. This again was found to be in a qualitatively good agreement with numerical and experimental data. Still, the comparison between the quantum results and the classical predictions being obtained by Fourier transforms of the quantum data, the accuracy is limited by the length of the available spectra (experimental or theoretical). For example, the imaginary part of the action of the complex orbit being given by the width of the corresponding peak in the Fourier transform, its exact value is hidden by the broadening of this peak. For the same reason, it is impossible to distinguish peaks closer one to each other than the “Fourier limit” as it is the case for the two orbits created at a bifurcation point.

In this paper, we show how an excellent agreement between the quantum and the semi-classical properties in the vicinity of a bifurcation can be obtained using the harmonic inversion, a newly developed method, which is able to bypass the Fourier limitation [19–21]. The paper is divided as follows : in section II the essential properties of the hydrogen atom in a magnetic field are given, then in section III we present the usual semi-classical approach of the saddle-node bifurcation. In section IV we briefly explain the harmonic inversion method, which is applied in section V to follow, from our quantum calculation, the properties of classical orbits through a saddle-node bifurcation.

## II. HYDROGEN ATOM IN MAGNETIC FIELD

In atomic units, the Hamiltonian of an hydrogen atom in a magnetic field is given by (using cylindrical coordinates) :

$$H = \frac{1}{2}\mathbf{p}^2 - \frac{1}{r} + \frac{1}{2}\gamma L_z + \frac{1}{8}\gamma^2 \rho^2 \quad (1)$$

where  $\gamma = B/B_0$ , with  $B_0 = 2.35 \times 10^5 T$ . Due to the rotational invariance around the  $z$ -axis of the Hamiltonian,  $L_z$  is a good quantum number and we shall take  $L_z = 0$  in what follows.

The classical counterpart of this Hamiltonian has a scaling property, that is, if we define new variables by :

$$\begin{cases} \tilde{\mathbf{r}} = \gamma^{2/3} \mathbf{r} \\ \tilde{\mathbf{p}} = \gamma^{-1/3} \mathbf{p} \\ \tilde{t} = \gamma t \end{cases} \quad (2)$$

we obtain a new Hamiltonian  $\tilde{H}$  given by :

$$\tilde{H} = \gamma^{-2/3} H = \frac{\tilde{\mathbf{p}}^2}{2} - \frac{1}{\tilde{r}} + \frac{\tilde{\rho}^2}{8}. \quad (3)$$

which does not depend anymore on  $\gamma$ . The classical dynamics of this Hamiltonian is entirely fixed by the scaled energy  $\epsilon$  given by :

$$\epsilon = \gamma^{-2/3} E. \quad (4)$$

All properties of the classical trajectories of the original Hamiltonian can be deduced from the scaled dynamics using the scaling transformation (2). For example, the action  $S$  of an orbit (i.e.  $\int \mathbf{p} \cdot \mathbf{d}\mathbf{q}$ ) is related to the reduced action  $\tilde{S}(\epsilon)$  (all quantities with  $\tilde{\phantom{x}}$  refer to the scaled Hamiltonian) by :

$$S(E, \gamma) = \gamma^{-1/3} \tilde{S}(\epsilon). \quad (5)$$

From the quantum point of view, this scaling introduces an effective  $\hbar$  value, which is easily seen on the scaled Schrödinger equation,  $\tilde{H}\psi = \epsilon\psi$ , for fixed scaled energy  $\epsilon$  :

$$\left( -\frac{\gamma^{2/3}}{2} \Delta_{\tilde{\mathbf{r}}} - \frac{1}{\tilde{r}} + \frac{\tilde{\rho}^2}{8} \right) \psi = \epsilon \psi. \quad (6)$$

Thus, the effective  $\hbar$  is given by  $\gamma^{1/3}$  and so at fixed value of the scaled energy  $\epsilon$ , the semi-classical limit is obtained when  $\gamma$  tends to 0.

### III. SEMI-CLASSICAL APPROACH AND SADDLE-NODE BIFURCATION

The semi-classical approximation of the photo-ionization cross-section  $\sigma(\gamma, E)$  is obtained by a generalization of the Gutzwiller trace formula [14,22] and has the following expression :

$$\sigma(\gamma, E) = \sigma_{\text{Coul}}(E) + \sigma_{\text{osc}}(\gamma, E). \quad (7)$$

$\sigma_{\text{Coul}}(E)$  is a smooth background term and corresponds to the Coulombic cross-section that would be obtained in the absence of a magnetic field and, for energies close to the ionization threshold  $E = 0$ ,  $\sigma_{\text{Coul}}(E)$  is almost independent from  $E$ , so that in first approximation

$\sigma_{\text{Coul}}(E) \approx \sigma_{\text{Coul}}(0)$ . The second term is the oscillatory part of the cross-section and is given as a sum over all orbits closing at the nucleus (and their repetitions) [15,16,23] :

$$\sigma_{\text{osc}}(\gamma, E) = \frac{4\pi\omega}{c} \sum_k A_k(\gamma, E) \sin(\phi_k(\gamma, E)), \quad (8)$$

$\omega$  being the photon frequency. Actually, looking at cross-section for energies close the ionization threshold (i.e.  $E = 0$ ),  $\omega = (E - E_i)/\hbar$  is almost given by the initial state energy  $-E_i$  and does not depend on the energy  $E$ . In the preceding formula, each amplitude  $A_k$  involves different classical quantities [24], among which the matrix element  $m_{12}$  of the monodromy matrix (i.e. the stability matrix restricted to deviations perpendicular to a closed orbit in the energy shell). More precisely,  $A_k$  has the following expression :

$$A_k = 2(2\pi)^{3/2} \sqrt{\sin\theta_i \sin\theta_f} \mathcal{Y}_m(\theta_i) \mathcal{Y}_m(\theta_f) \frac{1}{\sqrt{|m_{12}|}}, \quad (9)$$

where  $\theta_{i,f}$  are respectively the initial and final angles (at the nucleus) of the trajectory with the axis  $z$  of the magnetic field. The function  $\mathcal{Y}_m(\theta)$  depends only on the structure of the initial state and the polarization of the exciting light. Physically, it represents the angular distribution of the excited electron leaving the nucleus. Explicit expressions for excitation with  $\pi$ -polarized light from the  $n = 1$  (ground state) or  $n = 2$  are the following [15,23,25]:

$$\begin{aligned} |\psi_i\rangle = |1s0\rangle & \quad \mathcal{Y}_0(\theta) = -\pi^{-1/2} 2^3 e^{-2} \cos\theta \\ |\psi_i\rangle = |2s0\rangle & \quad \mathcal{Y}_0(\theta) = -(2\pi)^{-1/2} 2^8 e^{-4} \cos\theta \\ |\psi_i\rangle = |2p0\rangle & \quad \mathcal{Y}_0(\theta) = (2\pi)^{-1/2} 2^7 e^{-4} (4 \cos^2\theta - 1). \end{aligned} \quad (10)$$

The phase  $\phi_k$  is given by :

$$\phi_k = S_k(\gamma, E) - \frac{\pi}{2} \mu_k + \frac{\pi}{4}, \quad (11)$$

where  $S_k$  is the action of the closed orbit. The index  $\mu_k$  takes into account the different phase shifts occurring at conjugate points, at the nucleus and at the crossings of the  $z$ -axis. This index will be called Maslov index, even if it is not the usual one. More precisely, it is given by the following formula (for  $m = 0$ ) [15]:

$$\mu = \nu_0 + \nu_1 + \nu_2 + \nu_3, \quad (12)$$

where  $\nu_0$  is the number of conjugate points ( $m_{12} = 0$ ) along the closed orbit,  $\nu_1$  is the number of points at which the velocity vanishes (only for self retracing orbits),  $\nu_2$  is the number of crossings of the  $z$ -axis and  $\nu_3$  is the number of times that an orbit leaves and reaches the nucleus. The case of the orbit along the field (i.e. the  $z$ -axis) is special and requires a slight modification (for details, see [4,15]).

The singularity in the classical equations of motion due to the divergence of the Coulomb potential at  $\mathbf{r} = \mathbf{0}$  is regularized using the semi-parabolic coordinates ( $u = \sqrt{r+z}$ ,  $v = \sqrt{r-z}$ ), giving rise to the following effective classical Hamiltonian [25,26]:

$$h = \frac{1}{2} p_u^2 + \frac{1}{2} p_v^2 - \epsilon(u^2 + v^2) + \frac{1}{8} u^2 v^2 (u^2 + v^2) = 2. \quad (13)$$

One can show that, due to the potential shape, there is a deep analogy of the classical dynamics with the 4-disk problem [27–29] (i.e. the dynamics of a point particle moving freely in the  $(u, v)$  plane and bouncing elastically off the walls made by four disks at the corners of a square). In the magnetized hydrogen atom, the role of the 4 disks are played by the 4 potential hills between the valleys along the  $u$  and  $v$  axis. Thus, the coding scheme of the 4-disk can be directly used : the  $(u, v)$  plane is divided in four parts delimited by the coordinates axis and each part is labeled with a number  $\in \{1, 2, 3, 4\}$  (see Fig. 3). Then for each orbit, a sequence  $s_1 \dots s_n$  is built, corresponding to the sequence of bounces [30] made by this orbit. At large positive scaled energy (above  $\epsilon = 0.33$ ), it seems that this coding scheme works perfectly well [28]. At lower scaled energy, some sequences of symbols become forbidden (pruning takes place); in the region studied in this paper, the coding scheme is still quite efficient. It allows us to derive few properties like the Maslov indices  $\mu_k$  in a very simple way [27–29].

Using scaling properties of the classical dynamics, the oscillating part of the cross-section can be rewritten as :

$$\begin{aligned}\sigma_{\text{osc}}(\gamma, \epsilon) &= \frac{4\pi\omega}{c} \sum_k \gamma^{1/6} \sigma_k(\epsilon) \\ &= \frac{4\pi\omega}{c} \sum_k \gamma^{1/6} \tilde{A}_k(\epsilon) \sin\left(\gamma^{-1/3} \tilde{S}_k(\epsilon) - \frac{\pi}{2} \mu_k(\epsilon) + \frac{\pi}{4}\right).\end{aligned}\quad (14)$$

The scaled amplitudes  $\tilde{A}_k$  are functions of the scaled energy  $\epsilon$  only (except for the orbit along the field, which is varying like  $\gamma^{1/6}$ ). The exact expression is directly derived from equation (9) :

$$\tilde{A}_k(\epsilon) = 2(2\pi)^{3/2} \sqrt{\sin \theta_i \sin \theta_f} \mathcal{Y}_m(\theta_i) \mathcal{Y}_m(\theta_f) \frac{1}{\sqrt{|\tilde{m}_{12}(\epsilon)|}}. \quad (15)$$

Looking at formula (14) one can see that, by fixing the scaled energy  $\epsilon$  and doing the Fourier transform of  $\gamma^{-1/6} \sigma(\gamma, \epsilon)$  with respect to the variable  $\gamma^{-1/3}$ , one must obtain peaks at the scaled actions of the closed orbits : this is the well-known scaled spectroscopy [3].

However, the preceding approach fails in case of a saddle-node bifurcation at a given value  $\epsilon_c$  of the scaled energy. At the bifurcation, two orbits are created, but with  $\tilde{m}_{12}$  coefficients equal to 0 and thus the scaled amplitude  $\tilde{A}_k$  of the two orbits are infinite. This divergence can be regularized by a detailed study of the modifications induced in the trace formula by the bifurcation [18,25]. More precisely, the contribution to the oscillating part of the cross-section due to the orbits involved in the bifurcation becomes :

$$\begin{aligned}\gamma^{1/6} \sigma_k &= 2(2\pi)^{3/2} \sqrt{\sin \theta_i \sin \theta_f} \mathcal{Y}_m(\theta_i) \mathcal{Y}_m(\theta_f) \gamma^{1/9} \left(\frac{3\tilde{\sigma}}{2}\right)^{1/6} |\tilde{M}|^{-1/2} \\ &\quad \times Ai\left(\left(\frac{3\tilde{\sigma}}{2}\right)^{2/3} \gamma^{-2/9} (\epsilon_c - \epsilon)\right) \sin\left(\gamma^{-1/3} (\tilde{S}(\epsilon_c)) - \frac{\pi}{2} \mu^0\right),\end{aligned}\quad (16)$$

where  $Ai(z)$  is the Airy function [31],  $\tilde{\sigma}$  and  $\tilde{M}$  are defined by local expansion of  $\tilde{S}$  and  $\tilde{m}_{12}$  near the bifurcation, that is :

$$\begin{cases} \tilde{S}(\epsilon)_{\pm} = \tilde{S}(\epsilon_c) \pm \tilde{\sigma} (\epsilon - \epsilon_c)^{3/2} \\ \tilde{m}_{12}(\epsilon)_{\pm} = \pm \tilde{M} (\epsilon - \epsilon_c)^{1/2}, \end{cases}\quad (17)$$

where  $\pm$  refers to the pair of orbits born above the bifurcation. At fixed value of the scaled energy  $\epsilon > \epsilon_c$  and for very small values of  $\gamma$  which corresponds to the semi-classical limit, using the asymptotic behaviour of Airy function [31], one obtains :

$$\begin{aligned} \gamma^{1/6} \sigma_k &= \frac{4\pi\omega}{c} \gamma^{1/6} \tilde{A}_0(\epsilon) \sin \left( \gamma^{-1/3} (\tilde{S}(\epsilon)_-) - \frac{\pi}{2} (\mu^0 - \frac{1}{2}) \right) \\ &+ \frac{4\pi\omega}{c} \gamma^{1/6} \tilde{A}_0(\epsilon) \sin \left( \gamma^{-1/3} (\tilde{S}(\epsilon)_+) - \frac{\pi}{2} (\mu^0 + \frac{1}{2}) \right) \end{aligned} \quad (18)$$

with  $\tilde{A}_0(\epsilon)$  is given by :

$$\tilde{A}_0(\epsilon) = 2(2\pi)^{3/2} \sqrt{\sin \theta_i \sin \theta_f} \mathcal{Y}_m(\theta_i) \mathcal{Y}_m(\theta_f) \frac{1}{\sqrt{|\tilde{M}| |\epsilon - \epsilon_c|^{1/2}}} \quad (19)$$

recovering thus the usual semi-classical contribution of the two closed orbits created at the bifurcation.

Below the bifurcation and again using the asymptotic behaviour of Airy function [31], one obtains :

$$\gamma^{1/6} \sigma_k = \frac{4\pi\omega}{c} \gamma^{1/6} \tilde{A}_0(\epsilon) \sin \left( \gamma^{-1/3} \tilde{S}(\epsilon_c) - \frac{\pi}{2} \mu^0 \right) e^{-\gamma^{-1/3} \tilde{\sigma}(\epsilon_c - \epsilon)^{3/2}}. \quad (20)$$

The contribution does not vanish, even if it is exponentially decreasing when going away from the bifurcation or going to the semi-classical limit  $\gamma \rightarrow 0$ . It has exactly the same functional dependence than for a usual closed orbit, if one allows the action to become complex  $\tilde{S}(\epsilon) = \tilde{S}(\epsilon_c) - i\tilde{\sigma}(\epsilon_c - \epsilon)^{3/2}$ , which is nothing but the continuation of Eq. (17) across the bifurcation. In fact, it can be interpreted as the contribution of a “ghost” closed orbit, living in a complexified phase space [18,25].

#### IV. HARMONIC INVERSION

This method is a powerful tool to extract Fourier components (phase and amplitude) of a signal, with a better accuracy than one obtained by the usual Fourier transform, which is limited by the total length of the signal. Especially, this method is very well adapted to distinguish peaks closer than the Fourier resolution, provided that they are well separated from the other ones. A complete description of this method and some of its applications can be found in references [21,32,33].

Given a time signal  $c(t)$ , known in the interval  $[0, T]$  and for which we assume the following expression :

$$c(t) = \sum_{n=1}^N a_n e^{-i\omega_n t}, \quad (21)$$

where  $a_n$  and  $\omega_n$  are the unknown amplitudes and frequencies to be extracted from the signal.

Of course, these can be obtained using standard Fourier transform, but then the resolution is limited by the interval length  $T$ , adding an artificial width equal to  $2\pi/T$  to each Fourier peak. Especially, for frequencies closer one to each other than  $4\pi/T$ , their values does not correspond to the respective maxima in the Fourier spectrum, as one can see from the following simple example :

$$\begin{aligned} c(t) &= ae^{-i(\omega_0 + \frac{1}{2}\delta\omega)t} + be^{-i(\omega_0 - \frac{1}{2}\delta\omega)t} \\ &= ae^{-i\omega_+ t} + be^{-i\omega_- t} \end{aligned} \quad (22)$$

where  $a$  and  $b$  are real numbers. The modulus square of the time limited Fourier transform (i.e.  $f(\omega) = \int_0^T dt c(t)e^{i\omega t}$ ), is given by :

$$\begin{aligned} |f(\omega)|^2 &= a^2 T^2 \operatorname{sinc}^2(\omega - \omega_+) \frac{T}{2} + b^2 T^2 \operatorname{sinc}^2(\omega - \omega_-) \frac{T}{2} \\ &\quad + 2ab T^2 \cos(\omega_+ - \omega_-) \frac{T}{2} \operatorname{sinc}(\omega - \omega_+) \frac{T}{2} \operatorname{sinc}(\omega - \omega_-) \frac{T}{2} \end{aligned} \quad (23)$$

where the function  $\operatorname{sinc}(x)$  is the usual  $\sin(x)/x$ . As expected, it is only a function of  $\tilde{\omega} = \omega - \omega_0$  :

$$\begin{aligned} |f(\tilde{\omega})|^2 &= a^2 T^2 \operatorname{sinc}^2(\tilde{\omega} - \frac{1}{2}\delta\omega) \frac{T}{2} + b^2 T^2 \operatorname{sinc}^2(\tilde{\omega} + \frac{1}{2}\delta\omega) \frac{T}{2} \\ &\quad + 2ab T^2 \cos \delta\omega \frac{T}{2} \operatorname{sinc}(\tilde{\omega} - \frac{1}{2}\delta\omega) \frac{T}{2} \operatorname{sinc}(\tilde{\omega} + \frac{1}{2}\delta\omega) \frac{T}{2} \end{aligned} \quad (24)$$

For  $T$  large enough (i.e. much larger than  $T_0 = 2\pi/\delta\omega$ ), the two peaks of the Fourier transform are well separated and we are able to extract from this Fourier transform the right values of the two frequencies  $\tilde{\omega}_+ = \delta\omega/2$  and  $\tilde{\omega}_- = -\delta\omega/2$ . On the contrary, as one can see in Fig. 1, when  $T$  is of the order of  $2\pi/\delta\omega$ , the effective positions of the peaks are less and less well defined. Even for  $T = 4\pi/\delta\omega$  (i.e. theoretical Fourier resolution two times as small as  $\delta\omega$ ), the distance between the two peaks is enlarged by 20 percent. Furthermore, how this shift is distributed between the two peaks depends strongly of the relative amplitude  $a/b$ . For example if  $b$  is 5 times as small as  $a$ , then  $b$  is shifted by 85 percent of the total shift, whereas  $a$  is only shifted by 15 percent.

It becomes worse and worse as the number of frequencies in the signal increases, which shows that the usual Fourier transform is of little interest to extract accurate information from a limited signal. On the contrary, the harmonic inversion can bypass this Fourier limitation.

The main idea of the harmonic inversion is to construct an abstract evolution operator  $U(t)$  and an abstract initial state  $|\Phi_0\rangle$  such that  $c(t)$  is given by  $\langle \Phi_0 | U(t) | \Phi_0 \rangle$ , where  $\langle \cdot | \cdot \rangle$  is a complex symmetric inner product (i.e.  $\langle \psi |$  is just the transpose of  $|\psi\rangle$ , without complex conjugation). The eigenvalues of this operator are the  $e^{-i\omega_n t}$ , showing that  $U$  is not an unitary operator ( $\omega_n$  being generally complex). Then by diagonalizing its matrix representation in a suitable basis, it is possible to extract with a much higher accuracy than the Fourier limit these eigenvalues; the associated eigenvectors are then used to find the amplitudes  $a_n$ . One possible basis is a Krylov basis :  $|n\rangle = U(n\delta t) |\Phi_0\rangle$ , where  $\delta t$  is a short time interval and  $n$  is an integer ( $0 \leq n \leq N$ ,  $N$  defining the basis size). Thus, the matrix representation

is simply given by  $A_{nn'} = \langle n|U(\delta t)|n'\rangle = c((n + n' + 1)\delta t)$ . The basis vectors being not orthogonal ( $B_{nn'} = \langle n|n'\rangle = c((n + n')\delta t)$ ), one has to solve the symmetric generalized eigenvalues problem :

$$A|\phi\rangle = e^{-i\omega\delta t}B|\phi\rangle \quad (25)$$

However, this simplest basis choice is not satisfactory for efficient numerical purpose, because all coefficients in the matrices have the same order of magnitude, such that a eigenvector will have significant overlap with all basis states. Furthermore, all frequencies  $\omega_n$  are equally represented, which means that  $N$  has to be of the order of the total number of frequencies, which can be very large. For this reason, another basis, using the filtering properties of the Fourier transform is introduced. The choice of the basis is done by selecting an interval  $[\omega_{\text{inf}}, \omega_{\text{sup}}]$  in which one wants to extract frequencies. For frequencies  $\omega_j$  in this interval, one builds a new basis  $|\psi_j\rangle = \sum_n e^{in\omega_j\delta t}|n\rangle$ . From the signal  $c(t)$ , only frequencies in the interval will give significant contributions to the basis vectors. Thus, one can take a much smaller basis, of the order of the number of frequencies in this interval. Moreover, the matrix structure of the evolution operator in this basis is essentially banded, that is matrix coefficients are decreasing rapidly when going away from the diagonal. The expressions of the coefficients and other details about the numerical resolution of the new generalized eigenvalues problem can be found in [21,32,33].

A first test of this method is to apply it to the preceding example. The results are shown in Fig. 2. For both graphs, the continuous line is modulus of the usual Fourier transform divided by  $T$  and the vertical segments are the amplitudes given by the harmonic inversion. Sizes of the Krylov basis from 2 to 50 have been used, although 2 would have been enough, to emphasize that even when using an over-complete basis (which would be the standard case, as the number of frequencies is unknown) the results given by the harmonic inversion are not affected. The upper graph has been made for a signal length equal to  $T_0 = 2\pi/\delta\omega$ , i.e. the theoretical Fourier resolution is the distance between the two peaks. The bottom graph is made for a signal length  $T_0/10$ . From both pictures, it appears clearly that the harmonic inversion is much more efficient than the usual Fourier transform : for  $T = T_0$ , the Fourier transform still shows two peaks, but shifted by more than 20 percent from the exact positions and for  $T = T_0/10$ , the two peaks have collapsed in a single peak, whose width is much larger than  $\delta\omega$ .

On the contrary, values extracted by the harmonic inversion are very well localized, at the right frequencies. More precisely, the accuracy on different parameters (position and amplitude) are shown in table I. Of course, this example is rather simple, but even for signal length such that the Fourier resolution would be ten times as large as the peak separation and for relative amplitudes differing by two orders of magnitude, the accuracies are better than  $10^{-6}$  on the frequencies and  $10^{-5}$  on the amplitudes. For more complicated situations, the accuracy is expected to be worse than in the present example, but it will be still much better than what we would be able to extract from the Fourier transform.



## V. RESULTS

How one can apply the harmonic inversion in the case of the hydrogen atom in a magnetic field is obvious if one compares equations (21) and (14) :  $\gamma^{-1/3}$  corresponds to time  $t$ , the scaled action  $\tilde{S}_k(\epsilon)$  to (minus)  $\omega_n$  and  $\tilde{A}_k \exp\left(-i\frac{\pi}{2}\mu_k + i\frac{\pi}{4}\right)$  to  $a_n$ . For negative scaled energy  $\epsilon$ , the function  $\tilde{\sigma}(\gamma, \epsilon)$  is a just a sum of Dirac delta functions :

$$\tilde{\sigma}(\gamma, \epsilon) = \frac{4\pi\omega}{c} \sum_{n=0}^{\infty} \tilde{f}_n(\epsilon) \delta(\gamma^{-1/3} - \gamma_n^{-1/3}) \quad (26)$$

where  $\gamma_n^{-1/3}$  are the eigenvalues of the scaled quantum Hamiltonian (i.e.  $\epsilon$  being fixed, energy  $E$  quantization, because of equation (4), is equivalent to  $\gamma^{-1/3}$  quantization).  $\tilde{f}_n$  are the associated (squared) excitation matrix elements.

That we explicitly know the functional dependency of  $c(t = \gamma^{-1/3})$  can be used to simplify the implementation of the harmonic inversion. Indeed, the latter was written in the case of a general signal obtained either numerically or experimentally and known only at equally spaced values of time. On the contrary, in the present case, we are able to compute  $c(t)$  for any time  $t$ . A straightforward method would be to compute  $c(t)$  only on a grid. But because of  $\delta$  functions we would have to add an artificial width to each peak for numerical purpose, as it is done in ref [33]. The other way round is to modify a little bit the generalized eigenvalues problem (25), in which the matrix representation of the evolution operator  $U(t)$  was used, to obtain directly a generalized eigen-equation for the operator  $\Omega$ , defined by  $U(t) = e^{-i\Omega t}$ , which is very close to what was done in the original articles of Neuhauser [19,20]. If one writes the eigensystem in the following form :

$$\tilde{A}|\phi\rangle = -i\omega\tilde{B}|\phi\rangle \quad (27)$$

then the coefficients of  $\tilde{A}$  are given by :

$$\begin{aligned} \tilde{A}(\phi_1, \phi_2) = & \\ (\phi_1 \neq \phi_2) & \quad \frac{1}{\phi_1 - \phi_2} \left[ \phi_2 \int_0^{T/2} dt c(t) e^{it\phi_2} - \phi_1 \int_0^{T/2} dt c(t) e^{it\phi_1} \right. \\ & \quad \left. - \phi_2 e^{i\frac{T}{2}(\phi_1 - \phi_2)} \int_{T/2}^T dt c(t) e^{it\phi_2} + \phi_1 e^{i\frac{T}{2}(\phi_2 - \phi_1)} \int_{T/2}^T dt c(t) e^{it\phi_1} \right] \\ (\phi_1 = \phi_2) & \quad - \left[ \int_0^{T/2} dt c(t) e^{it\phi_1} + i\phi_1 \int_0^{T/2} dt c(t) t e^{it\phi_1} - \int_{T/2}^T dt c(t) e^{it\phi_1} \right. \\ & \quad \left. + iT\phi_1 \int_{T/2}^T c(t) e^{it\phi_1} - i\phi_1 \int_{T/2}^T dt c(t) t e^{it\phi_1} \right] \end{aligned} \quad (28)$$

where  $\phi_1$  and  $\phi_2$  are two frequencies taken in the interval  $[\omega_{\text{inf}}, \omega_{\text{sup}}]$  in which one wants to

extract the  $\omega_n$ . The matrix elements of  $\tilde{B}$  have similar expressions :

$$\begin{aligned} \tilde{B}(\phi_1, \phi_2) = & \\ (\phi_1 \neq \phi_2) & \quad \frac{i}{\phi_1 - \phi_2} \left[ \int_0^{T/2} dt c(t) e^{it\phi_2} - \int_0^{T/2} dt c(t) e^{it\phi_1} \right. \\ & \quad \left. - e^{i\frac{T}{2}(\phi_1 - \phi_2)} \int_{T/2}^T dt c(t) e^{it\phi_2} + e^{i\frac{T}{2}(\phi_2 - \phi_1)} \int_{T/2}^T dt c(t) e^{it\phi_1} \right] \\ (\phi_1 = \phi_2) & \quad \int_0^T dt c(t) e^{it\phi_1} \left( \frac{T}{2} - \left| \frac{T}{2} - t \right| \right) \end{aligned} \quad (29)$$

Insertion of signal (26) in the preceding expressions is straightforward and leads us to replace all integrals with sums on the available eigenenergies  $\gamma_n^{-1/3}$ .

Using the preceding implementation of the harmonic inversion, we will focus on the so-called X1 bifurcation [3], which is of the saddle-node type : at the bifurcation energy  $\epsilon_c = -0.11544216$ , two closed orbits are created, one stable and one unstable. The important point is that these two orbits have classical actions very well separated from all other closed orbits, so that their evolution with the scaled energy can be easily followed (both on the experimental and theoretical points of view).

All quantum properties (energy levels and excitation matrix elements) have been obtained by numerical diagonalization of sparse matrices, which are representations of the full Hamiltonian in sturmian basis (for further details see ref. [34]). Thus, for each value of the scaled energy  $\epsilon$ , we have  $\approx 10000$  eigenvalues, giving a length signal equal to  $\approx 120$ .  $\epsilon$  values are ranging from  $-0.15$  to  $-0.07$  with  $0.001$  step. For each scaled energy below  $\epsilon_c$ , the complex scaled action and the amplitude of the ghost peak have been extracted, whereas for scaled energy above  $\epsilon_c$ , actions of both real orbits created at the bifurcation and their amplitudes have been extracted.

To emphasize the agreement with the semi-classical formula (18) (20), we have also computed, for each value of the scaled energy, the classical quantities (scaled action, Lyapunov exponent and Maslov indices). For scaled energy below  $\epsilon_c$ , the ghost orbits are found by extending the classical equations of motion in complex plane, which also makes time to be complex. More precisely, for real closed orbits, one has to determine two parameters (i.e. the initial direction of the orbit and its time length), whereas for complex closed orbits one has to determine four parameters (i.e. the complex initial direction and the complex final time). However, integration for complex time requires to integrate along paths in the complex plane; it is far from obvious that the (complex) classical quantities are functions of the final time only. For simple systems, like a one-dimensional double well potential, one can show that the classical quantities are meromorphic functions of the final time, but to our knowledge, there is no exact proof in the case of the hydrogen atom in a magnetic field. Still, the potential being a polynomial function of the coordinates  $(u, v)$ , the structure of the equations of motion is such that the classical quantities are locally analytic, so that small deviations from a given path lead to the same results. Thus, even if a complete study of all singularities and branch points in the complex plane would be needed to justify this approach, one restricts integration of classical equations of motion on straight lines in the complex time plane starting from the origin, the integration time being simply the length along the line. In that case, the usual Runge-Kutta method can still be used. For example,

the ghost orbit associated with the X1 bifurcation is shown in Fig. 3(top). The scaled energy is  $\epsilon = -0.14$ . The continuous line is the real part, that is in the plane  $(\text{Re}(u), \text{Re}(v))$ , whereas the dotted line is the imaginary part (i.e. in the plane  $(\text{Im}(u), \text{Im}(v))$ ). On the bottom are shown the two real orbits (at scaled energy  $\epsilon = -0.11$ ) created at the bifurcation. The dashed line corresponds to the  $S_-$  orbit and the continuous line to the  $S_+$  orbit. The fact that the only difference between the two trajectories is the additional bounce (i.e. another conjugate point) in the  $(u > 0, v < 0)$  part of the space for the longest orbit ( $S_+$ ) explains that the Maslov indices associated with these orbits are  $\mu_- = \mu_0$  and  $\mu_+ = \mu_0 + 1$ . If we use the coding scheme of the 4-disk problem discussed above, the two orbits involved in the bifurcation have respectively codes 124 and 1214 (see Fig. 3), from which (using Eq. (12)) we calculate the Maslov indices  $\mu_0 = 8$  and  $\mu_0 + 1 = 9$ .

The first comparison is shown by Fig. 4 where scaled actions of the orbits are shown as functions of the scaled energy. Below the bifurcation (on the left), is shown the real part of the action and above the bifurcation (on the right), are shown the actions of the two orbits born at the bifurcation. The continuous lines are the classical calculation, whereas the circle are the values extracted from the quantum data. The agreement is excellent, even very close to the bifurcation point. This agreement is emphasized in Fig. 6, where on the left side, is shown the imaginary part of action of the ghost orbit, and, on the right side, is shown the difference  $\Delta S = (\tilde{S}_2 - \tilde{S}_1)/2\pi$ . Here again, the agreement is good, especially if one compares with the Fourier resolution which is  $\approx 0.0085$ . It shows clearly that it would have been impossible to extract the right behaviour of neither the width of the ghost peak nor the separation in the actions of the real orbits where it is the most interesting, that is as close as possible of the bifurcation. This clearly appears in Fig 5 where the usual Fourier transform, that is

$$|F(\epsilon, \tilde{S})| = \left| \int_0^{\gamma_{\max}^{-1/3}} d(\gamma^{-1/3}) \gamma^{-1/6} \sigma(\gamma, \epsilon) e^{-i\tilde{S}\gamma^{-1/3}} \right| \quad (30)$$

is drawn in the  $(\epsilon, \tilde{S}/2\pi)$ -plane. It is obvious that one can not distinguish the two orbits for scaled energy  $\epsilon$  closer to the bifurcation than  $\epsilon = -0.085$ . Furthermore, even if for scaled energy greater than  $-0.085$ , the two real orbits seem to be far enough one from each other to be seen on the Fourier transform, we know from the simple example shown in section IV that even for theoretical Fourier resolution twice better than the peaks separation, the extracted positions are still shifted by  $\approx 20$  percent. This tells us that quantitative comparison with the classical dynamics would have been possible only for scaled energy larger than  $-0.07$ . But at that point, other peaks corresponding to a family of orbits start to overlap with these two peaks, so that it would be hardly impossible to extract any quantitative information. Also, it would be difficult, at present time, to have a Fourier resolution twice better only by increasing the signal length : as the density of states is proportional to  $\gamma^{-1/3}$ , the number of states below a given  $\gamma^{-1/3}$  is proportional to  $\gamma^{-2/3}$ , and thus to obtain a signal length twice as long, one would have to compute more than 40000 levels, which is at the edge of the present numerical possibilities (i.e. it would require 32 times as much CPU time and 8 times as much memory).

After having compared the frequencies, one can compare the amplitudes with the semi-classical predictions. The results are shown in Fig. 7. The continuous lines are the individual

semi-classical amplitudes as obtained from equation (15), with the  $\mathcal{Y}_m$  function corresponding to transition from the  $|2s_0\rangle$  initial state, with  $\pi$ -polarized light (see equation (10)). On both sides of the bifurcation point  $\epsilon_c$ , two different regimes clearly appear. For  $|\epsilon - \epsilon_c| > 0.02$ , the agreement with the semi-classical prediction is quite good, even if not as good as for the actions. On the contrary for energies too close to the bifurcation point (i.e.  $|\epsilon - \epsilon_c| < 0.02$ ), the discrepancy is large, showing thus that the semi-classical approximation is no more valid. This can be easily understood from equation (16), which shows that the semi-classical limit (i.e.  $\gamma^{-1/3} \rightarrow +\infty$ ) is in competition with the limit  $\epsilon \rightarrow \epsilon_c$ . In other words, for fixed value of  $\gamma^{-1/3}$ , one goes out of the semi-classical limit when approaching the bifurcation. The break point corresponds to the argument of the Airy function of the order of one, which for  $\gamma^{-1/3} = 120$  (the largest available value) gives  $\epsilon - \epsilon_c \approx 0.01$ , in agreement with the results. For  $\epsilon > \epsilon_c$ , the argument of the Airy function being directly related to the separation in action  $\Delta\tilde{S}$  (see equation (17)), the preceding argument corresponds exactly to the fact that, for fixed scaled energy value, the phase shift  $2\pi\gamma^{-1/3}\Delta\tilde{S}$  has to be large enough ( $\gtrsim 2\pi$ ), so that the two orbits become distinguishable from the quantum point of view. A very simple test of the fact that we cannot use any asymptotic expansion of the Airy function, is to consider the amplitude exactly at the bifurcation point. In that case, the Airy function is only taken at the value 0, for any value of  $\gamma^{-1/3}$ . More precisely, the term  $B_{k_c} \sin\left(\gamma^{-1/3}\tilde{S}(\epsilon_c) - \frac{\pi}{2}\mu^0\right)$  in the oscillating part of the cross-section (see equation (16)) becomes :

$$\begin{aligned} \gamma^{1/6}\sigma_k = \frac{4\pi\omega}{c}\gamma^{1/9} 2(2\pi)^{3/2}\sqrt{\sin\theta_i\sin\theta_f}\mathcal{Y}_m(\theta_i)\mathcal{Y}_m(\theta_f)\left(\frac{3\tilde{\sigma}}{2}\right)^{1/6} \\ \times |\tilde{M}|^{-1/2}Ai(0)\sin\left(\gamma^{-1/3}\tilde{S}(\epsilon_c) - \frac{\pi}{2}\mu^0\right) \quad (31) \end{aligned}$$

From this equation, one can see that it is possible to extract the amplitude from the quantum data using harmonic inversion, provided that the signal is multiplied by  $\gamma^{-1/9}$ . For this purpose, 7000 levels have been computed at scaled energy  $\epsilon = \epsilon_c$ . The amplitude extracted from this data is 2.94, in a very good agreement with the theoretical value 2.951 given by equation (31).

Having compared the modulus of the amplitude, we now turn to its phase, i.e. Maslov indices. As the Maslov indices occur only in the phases with a multiplicative factor  $\pi/2$ , they can only be measured modulo 4. Fig. 8 shows the nice agreement between the Maslov indices extracted from harmonic inversion of the quantum signal and the semi-classical predictions. Indeed, from equation (18), the Maslov indices of the two real orbits ( $\epsilon > \epsilon_c$ ) are respectively  $\mu_0$  and  $\mu_0 + 1$  (with  $\mu_0 = 8$ , i.e. 0 modulo 4) whereas it is  $\mu_0$  for the ghost orbit ( $\epsilon < \epsilon_c$ ) which is exactly what is depicted by the figure. Exactly at the bifurcation point, with the modified harmonic inversion described in the previous paragraph, we obtain a Maslov index of 0.05, again in perfect agreement with the theoretical value  $\mu_0 = 0$  (modulo 4).

Even if the agreement between the different quantities is excellent, it is not as exceptional as in the simple example (22). The possible explanation comes from the fact that one assumes the expression for the signal to be a sum of exponentials with constant coefficients. This is clearly broken in the case of the semi-classical approximation because of the smooth contribution in either the density of state or the oscillator strength (i.e. Thomas-Fermi like terms) and also because of the remaining terms in the asymptotic expansion in  $\hbar$ . All this will contribute to (slowly) varying coefficients, which will make the harmonic inversion

method less efficient. This is clearly emphasized by the behaviour of the amplitudes for scaled energy too close to the bifurcation for which one cannot use anymore the asymptotic expansion of the Airy function.

## VI. CONCLUSIONS

In summary, we have shown that, using the harmonic inversion method, the properties (actions, Maslov indices and stabilities) of the classical orbits involved in the photo-ionization cross-section of the hydrogen atom in a magnetic field can be extracted with a much better accuracy than the usual Fourier transform, and this even for scaled energies close to a bifurcation point. Below the bifurcation, the contribution of a ghost orbit has been emphasized by showing that the behaviour of the imaginary part of its action is in perfect agreement with the classical predictions. For scaled energy above the bifurcation, we have been able to distinguish the contributions of the two orbits created at the bifurcation and we have also shown the perfect agreement with the semi-classical prediction for the frequencies, amplitudes and phases of the modulations. We have also emphasized the non-semiclassical behaviour of the amplitudes too close to the bifurcation point.

Laboratoire Kastler Brossel is laboratoire de l'Université Pierre et Marie Curie et de l'Ecole Normale Supérieure, unité mixte de recherche 8552 du CNRS. CPU time on a Cray C90 computer has been provided by IDRIS.

## REFERENCES

- [1] H. Friedrich and D. Wintgen, *Phys. Rep.* **183**, 37 (1989).
- [2] D. Delande in *Chaos and quantum physics*, edited by M.-J. Giannoni, A. Voros and J. Zinn-Justin, Les Houches Summer School, Session LII (North-Holland, Amsterdam, 1991).
- [3] A. Holle, J. Main, G. Wiebusch, H. Rottke, and K.H. Welge, *Phys. Rev. Lett.* **61**, 161 (1988).
- [4] J. Main, G. Wiebusch, K. Welge, J. Shaw and J.B. Delos, *Phys. Rev. A* **49**, 847 (1994).
- [5] M. Domke, K. Schulz, G. Remmers, A. Gutiérrez, G. Kaindl, and D. Wintgen, *Phys. Rev. A* **53**, R4309 (1995).
- [6] R. Püttner, B. Grémaud, D. Delande, M. Domke, M. Martins, A.S. Schlachter, and G. Kaindl (to be published).
- [7] P.M. Koch and K.A.H. van Leeuwen, *Phys. Rep.* **255**, 289 (1995).
- [8] J.E. Bayfield, *Chaos* **1**, 110 (1991).
- [9] T.M. Fromhold *et al*, *Phys. Rev. Lett.* **72**, 2608 (1994).
- [10] G. Muller, G.S. Boebinger, H. Mathur, L.N. Pfeiffer, and K.W. West, *Phys. Rev. Lett.* **75**, 2875 (1995).
- [11] D.S. Saraga and T.S. Monteiro, *Phys. Rev. Lett.* **81**, 5796 (1998).
- [12] F.L. Moore, J.C. Robinson, C. Bharucha, P.E. Williams, and M.G. Raizen, *Phys. Rev. Lett.* **94**, 2974 (1994).
- [13] B.G. Klappauf, W.H. Oskay, D.A. Steck, and M.G. Raizen, *Phys. Rev. Lett.* **81**, 4044 (1998).
- [14] *Chaos in Classical and Quantum Mechanics* M.C. Gutzwiller (Springer, New York, 1990).
- [15] E.P. Bogomolny, *Zh. Eksp. Teor. Fiz.* **96**, 487 (1989) [*Sov. Phys. JETP* **69**, 275 (1989)].
- [16] J. Gao and J.B. Delos, *Phys. Rev. A* **46**, 1455 (1992).
- [17] J.M. Mao and J.B. Delos, *Phys. Rev. A* **45**, 1746 (1992).
- [18] M. Kuś, F. Haake and D. Delande, *Phys. Rev. Lett.* **71**, 2167 (1993).
- [19] D. Neuhauser, *J. Chem. Phys.* **93**, 2611 (1990).
- [20] M.R. Wall and D. Neuhauser, *J. Chem. Phys.* **102**, 8011 (1995).
- [21] J. Main, V.A. Mandelshtam and H.S. Taylor, *Phys. Rev. Lett.* **79**, 825 (1997).
- [22] Gaspard P., Alonso D., and Burghardt I. *Adv. Chem. Phys.* **XC** 105 (1995).
- [23] M.L. Du and J.B. Delos, *Phys. Rev. A* **38**, 1896 (1988); **38**, 1913 (1988).
- [24] J.M. Mao, J. Shaw and J.B. Delos, *J. Stat. Phys.* **68**, 51 (1992).
- [25] J. Main and G. Wunner, *Phys. Rev. A* **55**, 1743 (1997).
- [26] *Group Theory and the Coulomb Problem* M.J. Englefield (Wiley, New York, 1972).
- [27] B. Eckhardt and D. Wintgen, *J. Phys. B: At. Mol. Opt. Phys.* **23**, 355 (1990).
- [28] K.T. Hansen, *Phys. Rev. E* **51**, 1838 (1995).
- [29] G. Tanner, K.T. Hansen and J. Main, *Nonlinearity* **9**, 1641 (1996).
- [30] For the magnetized hydrogen atom, these bounces are “soft” bounces on the potential hills, which, as shown in [28], can be associated with zeros of the matrix element  $m_{12}$  of the monodromy matrix.
- [31] *Handbook of Mathematical Functions*, edited by M. Abramovitz and I.A. Stegun (Dover, New York, 1965).

- [32] V.A. Mandelshtam and H.S. Taylor, *J. Chem. Phys.* **107**, 6756 (1997).
- [33] J. Main, V.A. Mandelshtam, G. Wunner and H.S. Taylor, *Nonlinearity* **11**, 1015 (1998).
- [34] R. Marcinek and D. Delande (to be published).

## FIGURES

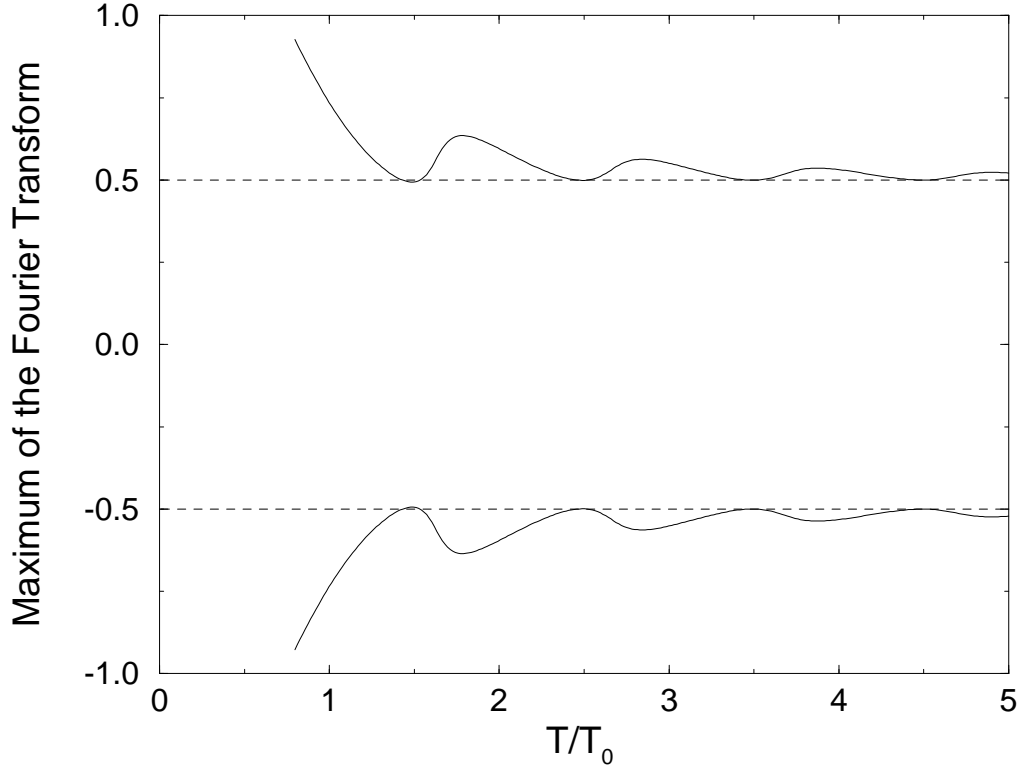


FIG. 1. Effective frequencies extracted from the signal  $c(t) = \exp(i\delta\omega t/2) + \exp(-i\delta\omega t/2)$  using finite Fourier transform, i.e.  $\int_0^T dt c(t) \exp(i\tilde{\omega}t)$ , as functions of  $T$ . For large values of  $T$  (much larger than  $T_0 = 2\pi/\delta\omega$ ) we recover the right values of  $\tilde{\omega}$ , that is  $\pm\delta\omega/2$  (dashed lines). On the contrary, for  $T$  of the order of  $T_0$ , the frequencies given by the Fourier transform are substantially shifted from the correct values. For example, for  $T = 2T_0$ , the distance between the two peaks is enlarged by 20 percent.



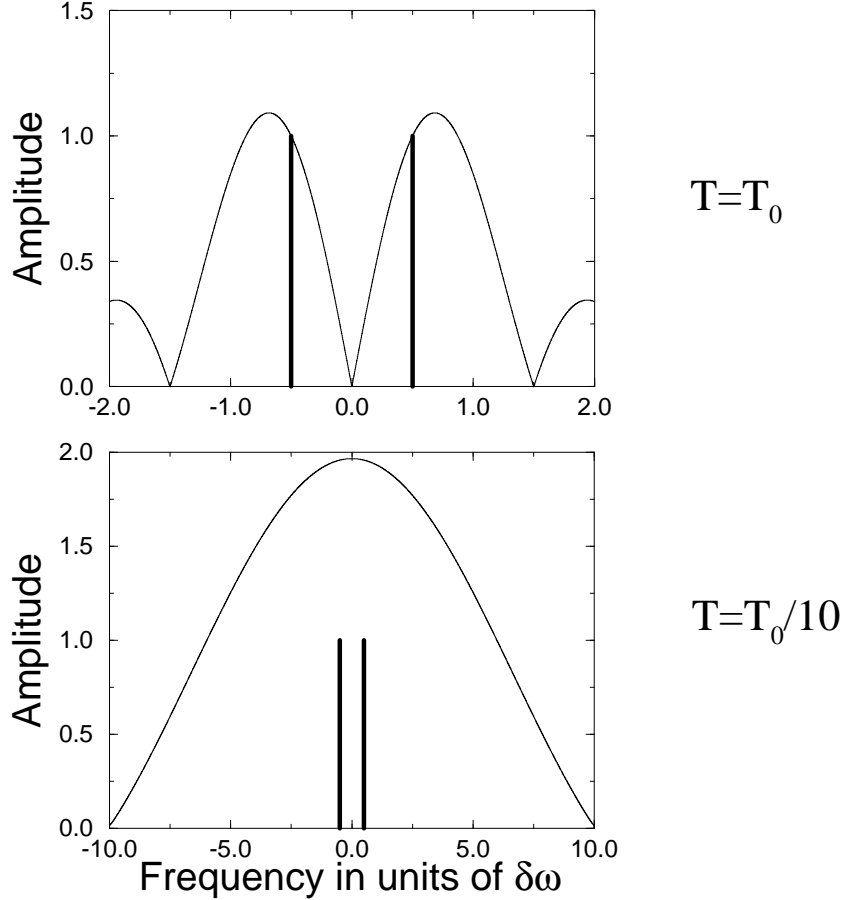


FIG. 2. Comparison between the usual Fourier transform and the harmonic inversion technique for the signal  $c(t) = \exp(i\delta\omega t/2) + \exp(-i\delta\omega t/2)$ . For both graphs, the continuous line is the usual Fourier transform  $|F(T)|/T$  ( $T$  is the length of the available signal  $c(t)$ ), whereas the vertical lines are at the frequencies given by the harmonic inversion, their heights corresponding to the associated amplitude (also obtained by harmonic inversion). The upper graph is made for  $T = T_0 = 2\pi/\delta\omega$ , which means that the Fourier resolution is of the order of the peak separation. Again, we recover the fact that the effective positions given by the Fourier transform are quite shifted from the exact values and the amplitudes are also not correct. On the contrary, all values (amplitudes and positions) given by the harmonic inversion are in a perfect agreement. The lower graph is made for  $T = T_0/10$ , i.e. the Fourier resolution is 10 times as large as the peak separation, so that the Fourier transform is almost constant in the interval  $[-1, 1]$  and thus gives no information on the position of the peaks. In contrast, the harmonic inversion method is still working, with a very good accuracy (better than  $10^{-7}$ ).

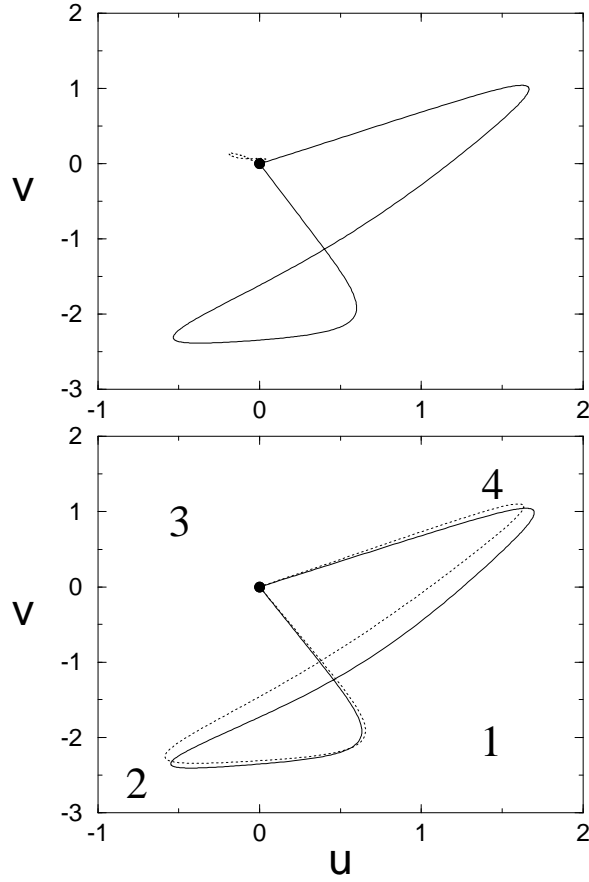


FIG. 3. Closed trajectories of the electron of an hydrogen atom in a magnetic field in the  $(u, v)$  (semi-parabolic coordinates) configuration space. On the top is shown the complex ghost orbit associated with the X1 peak experimentally observed in the scaled spectroscopy of the hydrogen atom in a magnetic field at scaled energy  $\epsilon = -0.14$  [3]. The continuous line is the real part of the trajectory, whereas the dotted line is the imaginary part. Eventually, this complex trajectory collapses with its complex conjugate in a saddle-node bifurcation at  $\epsilon_c = -0.11544216$ , from which two real orbits are created, shown on the bottom at scaled energy  $\epsilon = -0.11$ . The dashed line corresponds to the  $S_-$  orbit created at the bifurcation, whereas the continuous line corresponds to the  $S_+$  orbit. From this plot, one can easily deduce the code of each orbit, that is the sequence of bounces in the different quarters of space (1,2,3,4) defined by the coordinate axis : for  $S_-$ , the code is 124 and 1214 for  $S_+$  (one additional bounce on the  $(u > 0, v < 0)$  part of the plane).

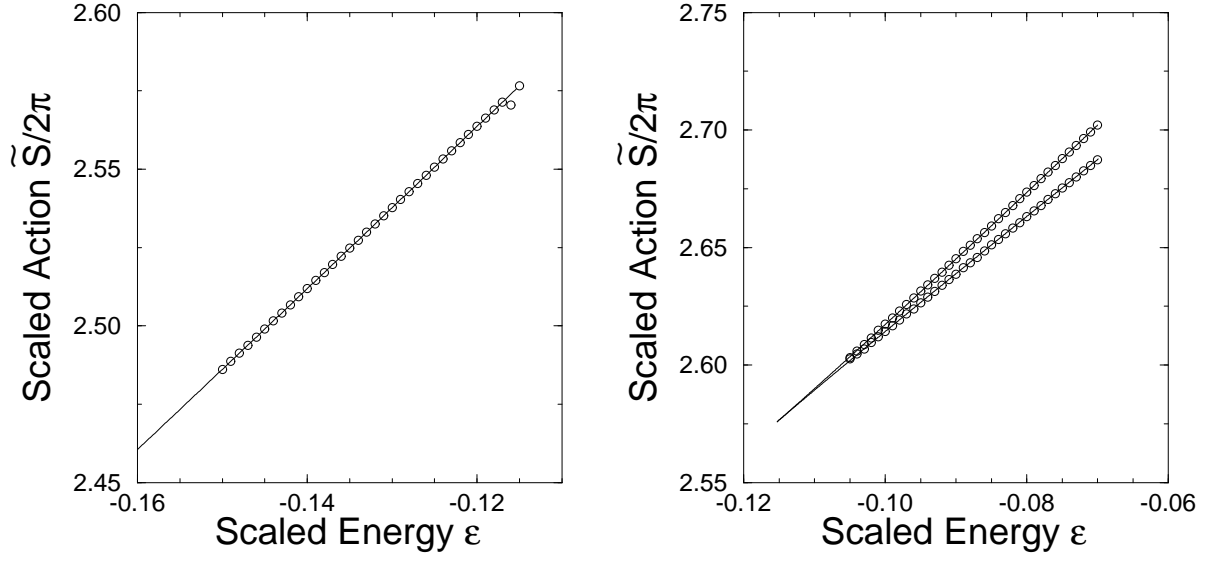


FIG. 4. Real part of the scaled actions as function of the scaled energy  $\epsilon$ . The continuous lines are the classical results, whereas circles are extracted from the quantum dynamics using harmonic inversion. One can follow the two real orbits born at the saddle-node bifurcation, even for separation much smaller than the standard Fourier limitation ( $\approx 0.01$ ).

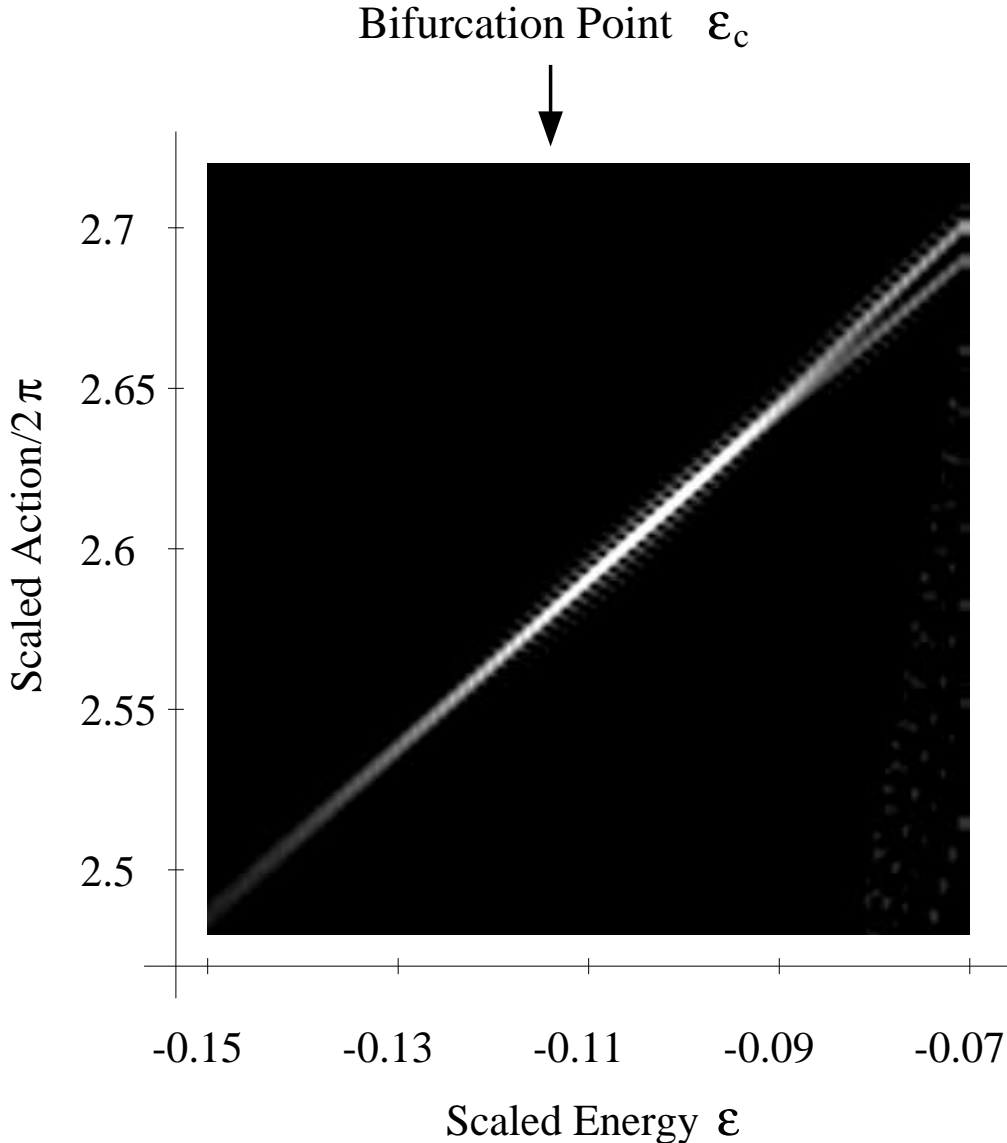


FIG. 5. Usual scaled Fourier transform (see equation (30)) of the photo-excitation cross-section of the hydrogen atom in a magnetic field, in the  $(\epsilon, \tilde{S}/2\pi)$ -plane. Below the bifurcation  $\epsilon_c = -0.11544216$ , one clearly sees the contribution of the ghost orbit. However, it would be very hard to extract the relevant information about the complex orbit, namely the imaginary part of the action, from the width of the peak. Especially, it should vanish like  $(\epsilon_c - \epsilon)^{3/2}$  near the bifurcation, which is not the case in the figure. Actually, it is dominated by the broadening due to the limited range of the Fourier transform. Above the bifurcation, the actions of the two real orbits created at the bifurcation are separated by the same power law. But the separation cannot be observed on this plot below  $\epsilon \approx -0.085$ , which is already too far from the bifurcation point to observe this power law.

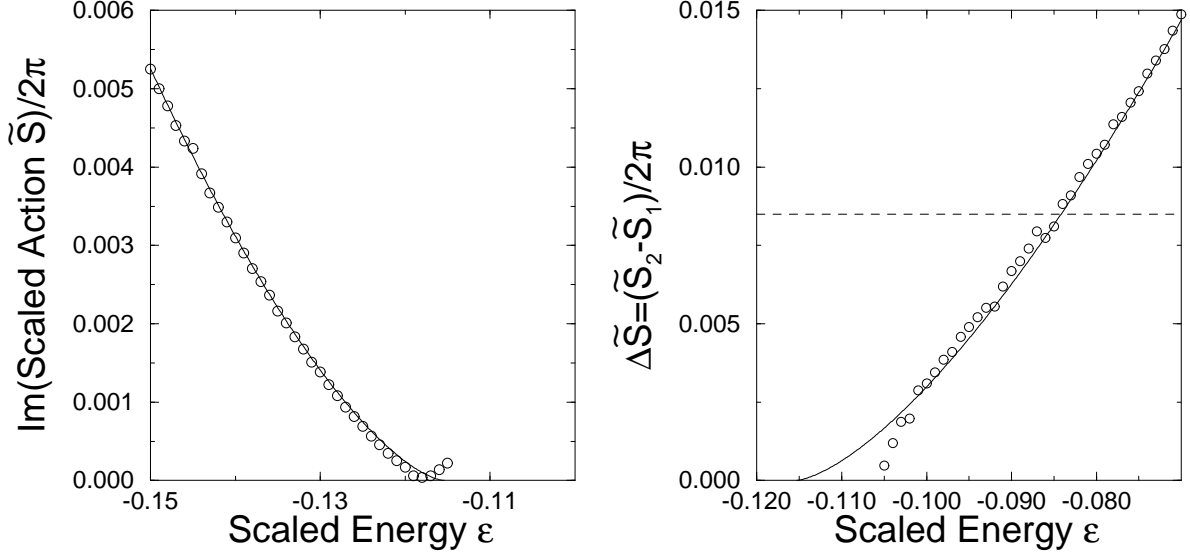


FIG. 6. On the left is the imaginary part of the scaled action of the ghost orbit (below the bifurcation) and on the right is the separation in action between the two real orbits above the bifurcation. For both graphs, we include levels up to  $\gamma_{\max}^{-1/3} = 120$ , so that the theoretical Fourier limitation would be  $\approx 8.5 \times 10^{-3}$ , but (see text), the actual resolution is at least twice as large. On the contrary, as it appears clearly on both figures, the limitations of the harmonic inversion are much smaller, which allows us to emphasize the good agreement between the semi-classical predictions and the exact quantum results.

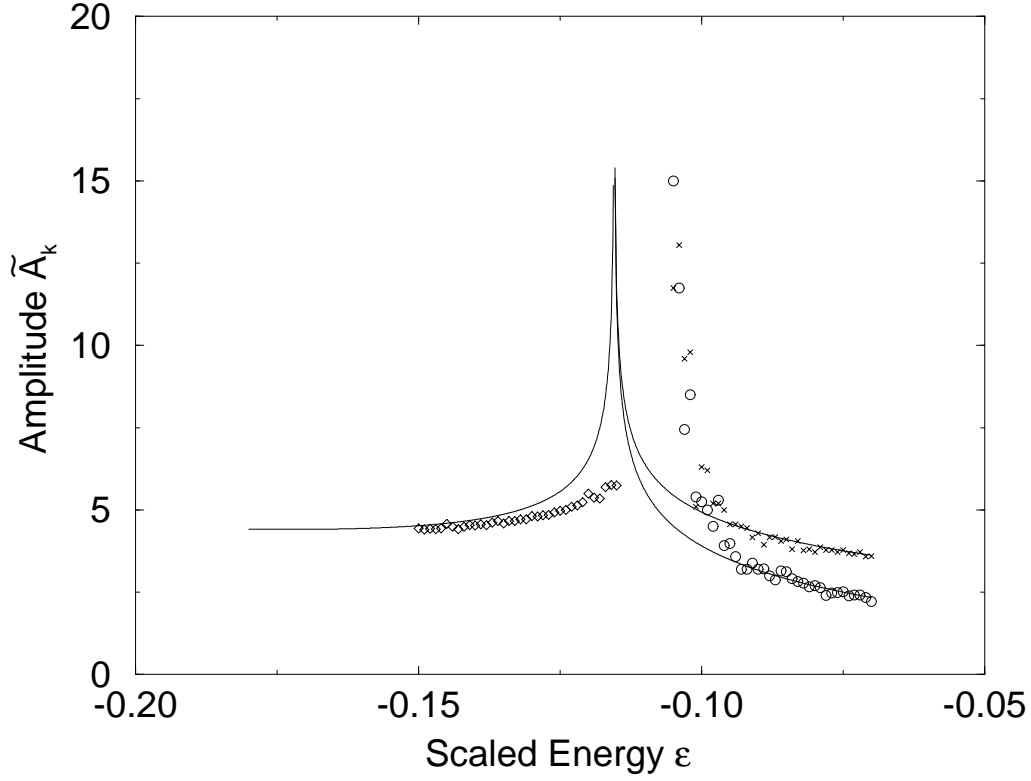


FIG. 7. Comparison of quantum amplitudes  $\tilde{A}_k(\epsilon)$  (see equations. (14) (15)) extracted using the harmonic inversion, with the semi-classical prediction. The continuous lines are the amplitudes calculated from the classical quantities (stability, initial and final angle). Diamond (ghost orbit), crosses and circles (real orbits) are the amplitudes extracted from the exact quantum results. On both sides of the bifurcation, two regimes appear. For scaled energy away enough from the bifurcation ( $|\epsilon - \epsilon_c| > 0.02$ ) the semi-classical predictions and the quantum results agree well. On the contrary for scaled energy too close to the bifurcation point, the deviation is large.

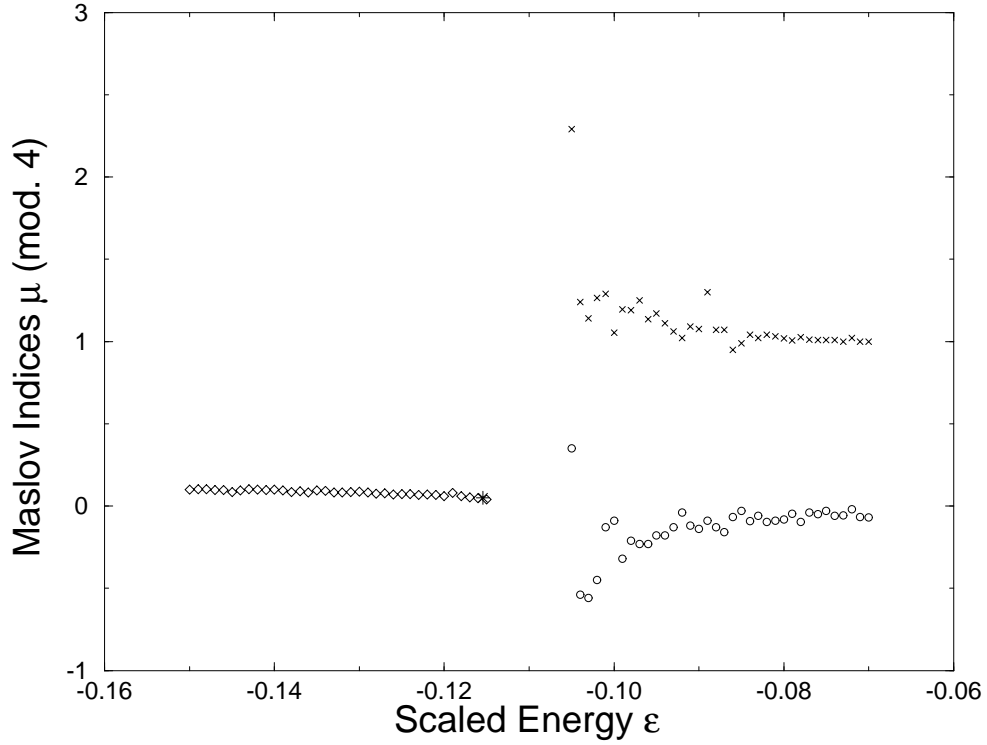


FIG. 8. Maslov indices (see equation (12) in text) associated with each orbit extracted from the exact quantum results. Above the bifurcation point  $\epsilon_c$ , we recover the semi-classical prediction that Maslov indices of the two real orbits created in a saddle-node bifurcation are  $\mu_0$  and  $\mu_0 + 1$ , where  $\mu_0$  is also the Maslov index of the ghost orbit. Furthermore, this value  $\mu_0 = 0$  (modulo 4) agrees with the one obtained from Eq. ((12)), giving  $\mu_0 = 8$ . The symbol (+) correspond to the  $\mu_0$  value extracted exactly at the bifurcation point, using a specific harmonic inversion technique (see text), also in perfect agreement with the theoretical predictions.

TABLES

TABLE I. Accuracy on parameters extracted from  $c(t) = a_0 e^{-i(\omega_0 + \delta\omega/2)t} + b_0 e^{-i(\omega_0 - \delta\omega/2)t}$  using harmonic inversion, for signal length  $T = 10T_0$ ,  $T = T_0$  and  $T = T_0/10$ , where  $T_0 = 2\pi/\delta\omega$ . This table emphasizes the excellent accuracy of the method. For  $T > T_0$ , it is of the order of the machine precision. For signal length ten times as short as the theoretical Fourier resolution, the accuracy is still of the order of  $10^{-7}$  on the frequency positions and  $10^{-6}$  on the amplitudes. Even for very peculiar situations (one peak 100 times as small as the other one and signal length 10 times as short as the theoretical Fourier resolution), the accuracy is still very good.

$a_0 = b_0$	$ \omega_+ - \omega_+^0 /\omega_+^0$	$ \omega_- - \omega_-^0 /\omega_-^0$	$ a - a_0 /a_0$	$ b - b_0 /b_0$
$T = 10T_0$	$< 10^{-14}$	$< 10^{-14}$	$< 10^{-14}$	$< 10^{-14}$
$T = T_0$	$\lesssim 10^{-13}$	$\lesssim 10^{-13}$	$\lesssim 10^{-12}$	$\lesssim 10^{-12}$
$T = T_0/10$	$\lesssim 10^{-7}$	$\lesssim 10^{-7}$	$\lesssim 10^{-6}$	$\lesssim 10^{-6}$
$100a_0 = b_0$				
$T = 10T_0$	$< 10^{-14}$	$< 10^{-14}$	$< 10^{-14}$	$< 10^{-14}$
$T = T_0$	$\lesssim 10^{-12}$	$\lesssim 10^{-14}$	$\lesssim 10^{-11}$	$\lesssim 10^{-13}$
$T = T_0/10$	$\lesssim 10^{-6}$	$\lesssim 10^{-8}$	$\lesssim 10^{-5}$	$\lesssim 10^{-7}$